energies

MDPI

Article

Mixed-Combustion Characteristics and Reaction Kinetics of Municipal Sludge and Corn Straw in Micro-Fluidized Bed

Shengjie Guo [1], Jinhui Tan [2], Zhongguo Yang [1], Shuhui Deng [1], Yaxuan Wang [1] and Shuai Guo [2,*]

[1] College of Civil Engineering and Water Resources, Heilongjiang Bayi Agricultural University, Daqing 163319, China; sjguo@byau.edu.cn (S.G.); yzg111402@byau.edu.cn (Z.Y.); dsh@cau.edu.cn (S.D.); wangyaxuan1980@byau.edu.cn (Y.W.)

[2] School of Energy and Power Engineering, Northeast Electric Power University, Jilin 132012, China; 2202000471@neepu.edu.cn

* Correspondence: shuaiguo@neepu.edu.cn; Tel.: +86-432-6480-6281

Abstract: With economic development, the output of municipal sludge (MS) continues to increase, and the effective utilization of corn straw (CS) also plays an important role in promoting "carbon neutrality". The mixed combustion of solid wastes is a very environmentally friendly technology; however, little research has occurred regarding the combustion characteristics and reaction kinetics of MS and CS in a fluidized bed. Therefore, this study used a micro-fluidized bed and process mass spectrometer to evaluate the mixed-combustion characteristics of MS and CS and analyze the effects of the temperature and mixing ratios on the reaction rate. Isothermal kinetics were used to calculate the activation energy, pre-exponential factors, and other kinetic parameters of this reaction. The results showed that with an increasing reaction temperature, the combustion reaction rate of MS and CS under different mixing ratios increased. The reaction rate of mixed combustion of MS and CS was greater than that of MS or CS alone. Compared with the homogeneous model, the shrinking core model is more suitable for analyzing the mixed-combustion behavior of MS and CS. The calculated activation energies of the mixed combustion in different proportions were lower than that of single fuel combustion. When the ratio of MS to CS was 2:8, the activation energy required for the reaction was minimum (28.00 kJ/mol), the pre-exponential factor was 9.06, and the fitting degree was larger than 0.99, which proved the reliability of the results.

Keywords: municipal sludge; corn straw; mixed combustion; carbon conversion rate; isothermal reaction kinetics; micro-fluidized bed

Citation: Guo, S.; Tan, J.; Yang, Z.; Deng, S.; Wang, Y.; Guo, S. Mixed-Combustion Characteristics and Reaction Kinetics of Municipal Sludge and Corn Straw in Micro-Fluidized Bed. *Energies* **2022**, *15*, 2637. https://doi.org/10.3390/en15072637

Academic Editor: Dino Musmarra

Received: 11 March 2022
Accepted: 1 April 2022
Published: 4 April 2022

1. Introduction

Social development has led to various issues related to fossil fuels such as resource shortages and environmental pollution [**?**]. With economic development, the amount of sewage discharge is increasing; municipal sludge (MS), as a secondary pollutant, has not been treated over time, resulting in environmental pollution. Incineration can be used to produce energy from MS while it is converted into harmless materials, therefore, it could be stabilized, reduced, and recycled after incineration [**?**]. China shows high potential for biomass energy utilization [**?**]. The biomass produced every year is equivalent to hundreds of millions of tons of standard coal. Therefore, biomass energy is an important factor in diversifying a country's energy structure [**?**]. Corn straw (CS) has certain representativeness and rich yield. Biomass is not only an important renewable resource but is also carbon-neutral, which is of great significance for carbon neutralization [**?**].

The development of biomass combustion technology is important for achieving the sustainable development of energy, the environment, and the economy. Single biomass combustion has various limitations, such as low calorific value, difficulty to burn, and ease of slag. Mixed burning may improve the combustion characteristics of biomass for

energy production [**?**]. Because biomass and MS have different basic characteristics, their mixed-combustion properties differ from those of the primary materials [**?**].

At present, relevant scholars have conducted a great deal of research work on mixed-combustion behaviors, pollutant-releasing characteristics, and reaction kinetics of biomass, coal, and municipal solid waste [**?** **?**]. Wang et al. [**?**] investigated the combustion behaviors of biomass, coal, and their mixtures via the thermogravimetric (TG) method. The results showed that both the ignition and burnout temperatures of the blends decreased as the biomass mixing ratio increased, while the ignition and flammability indexes increased. Qian et al. [**?**] explored the feasibility of electricity production with low emissions during the poultry litter and natural gas co-combustion process using a lab-scale advanced swirling fluidized bed combustion system. It was found that the emissions of SO_2 and NO_x could be reduced under appropriate conditions and also confirmed that poultry manure can be regarded as an energy source. Ryu et al. [**?**] studied the fixed-bed combustion of biomass samples with different particle types and properties. The results showed that the fuel type, equivalence ratio, and particle size were all significant factors impacting the mixed-combustion process. Wang et al. [**?**] conducted coal/biomass co-combustion experiments in a 0.1 MW oxy-fuel circulating fluidized-bed combustor and found that the mixed-fuel combustion of coal/biomass is able to realize negative CO_2 emission. Qin et al. [**?**] conducted combustion experiments of oil shale sludge and semicoke on TG to study the mechanism of co-combustion involved. The synergistic effect of sludge and semicoke was assessed using the interaction coefficient and the relative error of the mean square root. The results show that, during combustion, the synergistic behavior is different according to the variation of heating rates, as well as the mixing proportion. Yin et al. [**?**] studied the combustion kinetics of corn straw, papermaking sludge, and their mixtures via TG analysis. The comprehensive combustion characteristic index decreases with an increase in the mixing ratio of paper sludge in the blends and rises with an increased heating rate. Significant interactions occur in the mixed-combustion process. Wang et al. [**?**] carried out a mixed-combustion test of biomass and coal char at different ratios in a high-temperature thermogravimetric analyzer. The results show that with the increase in the biomass mixing ratio, both the ignition and combustion temperatures of the mixed fuel decrease, and the maximum combustion rate, average combustion rate, and comprehensive combustion characteristic index increase. The activation energy of the low-temperature section rises, and the activation energy of the high-temperature section declines continuously. Tian and Liao [**?**] examined a mixed fuel of coal, low-quality fuel oil shale, and high-sulfur fuel petroleum coke using the TG-differential thermal analysis method and differential subtraction methods. The mixed-combustion characteristic curve and mechanism were analyzed, and various burning parameters and combustion kinetic parameters of the sample were calculated. At an appropriate mixing ratio of coal, oil shale, and petroleum coke, the mixed-combustion characteristics were better than those of oil shale or petroleum coke alone. Dai et al. [**?**] used a TG analyzer to evaluate the combustion performance and dynamic characteristics of mixed samples of coal gangue and coal in different mass ratios. As the proportion of coal in the mixed sample increased, the ignition temperature and burnout temperature were reduced, the comprehensive combustion characteristic index increased, and the ignition and combustion characteristics were improved.

The above results show that mixed combustion of some combustibles may improve fuel performance. However, the mixed-combustion characteristics and reaction kinetics of MS and CS have not been widely examined, and recent studies of mixed combustion have mostly used the TG analysis method. The reaction is greatly affected by heat and mass transfer, and the intrinsic reaction process cannot be realized, leading to deviations from the calculation results of kinetic parameters. Therefore, in this study, we investigated the mixed-combustion process of CS and MS at different mixing ratios using a micro-fluidized bed reactor coupled with a process mass spectrometer, which can greatly reduce the reaction delay caused by product diffusion during the reaction; that is, the reaction tends to be dynamic, and thus intrinsic kinetic parameters can be obtained [**?**]. The effects

of temperature and the blending ratio on carbon conversion and the reaction rate were analyzed. Isothermal kinetics were used to calculate the kinetic parameters, and the best blending ratio of CS and MS was also determined.

2. Materials and Methods

2.1. Test Sample

MS was obtained from Huanjia Environmental Protection Co., Ltd., Dalian, China, while CS was selected from corn fields around Jilin City, Jilin Province, China. The raw materials were dried in a drying oven at 105 °C for 24 h and then pulverized. The pulverized raw materials were sieved through a 200-mesh sieve, mixed at different MS ratios (0%, 20%, 40%, 60%, 80%, and 100%), stirred with a small stick at a uniform speed for more than 30 min until the sample was fully mixed, and placed in a constant-temperature drying box for storage.

An automatic ultimate analyzer from (EA3000, Euro Vector, Pavia, Italy) was used for the element analysis of the samples, and the proximate analysis was performed based on the GB/T 28731—2012 Proximate analysis of solid biofuels. The results are shown in Table **??**. In the proximate analysis of CS, volatile matter accounted for the largest percentage, reaching as high as 76.56%. After the volatile matter was precipitated from inside of CS, it became porous and easier to burn. In the ultimate analysis of MS, the carbon content was 18.03%, which is less than that of CS, and MS could ignite and burn more easily. The nitrogen and sulfur contents of CS were 0.92% and 0.28%, respectively, with low nitrogen and sulfur contents, indicating that these materials are a form of clean energy. Besides, a 0.1 g sample was weighed and digested by microwave with 5 mL HNO_3 + 2 mL HF + 1 mL HCl. The contents of the typical heavy metal concentrations were determined by an inductively coupled plasma-mass spectrometer (ICP-MS) produced by Jiangsu Tianrui Instrument Co., Ltd., Kunshan, China [**?**]. The results are shown in Table **??**.

Table 1. The proximate analysis and ultimate analysis of test samples.

Sample	Proximate Analysis/W_{ad}%				Ultimate Analysis/W_{ad}%				
	M	**A**	**V**	**FC**	**C**	**H**	**O**	**N**	**S**
MS	3.84	58.80	32.66	4.70	18.03	2.85	76.45	2.07	0.60
CS	4.81	5.41	76.56	13.22	48.73	6.65	43.42	0.92	0.28

Note: ad = air dry basis; M: Moisture content; A: Ash content; V: Volatile matter; FC: Fixed carbon; C: Carbon; H: Hydrogen; O: Oxygen; N: Nitrogen; S: Sulfur.

Table 2. Concentration analysis of heavy metal in raw materials ($mg \cdot kg^{-1}$) (Adapted from ref. [**?**]).

Sample	As	Cr	Hg	Ni	Cu	Zn	Sb	Pb
MS	44.60	227.87	35.24	52.21	104.83	1158.88	3.74	41.72
CS	221.86	6.36	0.07	3.63	6.14	314.01	1.53	5.75

2.2. Test Device and Method of Operation

The experimental system of isothermal rapid combustion performed in a micro-fluidized bed can be divided into three parts: A fluidized bed carrier gas supply system, a fluidized bed combustion generator, and a gas production collection and analysis system, as shown in Figure **??**.

The fluidization gas in the experiment was argon, the bed material of the fluidized bed was quartz sand (particle size of 200–300 μm), the mass of the bed material was approximately 3.0 g, and the time of each electromagnetic pulse was set to 10 ms. The selected test temperature was 550–750 °C and the interval was 50 °C. Briefly, the bed material was added from the feed port, the reactor was placed in the heating furnace, the feed tube containing the sample was connected and fixed, and then the thermocouple was inserted to measure the temperature of the fluidization zone. We ensured that the fluidized bed was airtight. The combustion temperature was set by the software. After

beginning the heating process, the fluidization gas was introduced to cause the quartz sand to reach the fluidization state. After the preset temperature was reached, the pulse valve was opened, and the sample was blown into the main reaction zone that reached the fluidization state through the feed tube and mixed with the bed material quartz sand. The ratio between the quartz sand and reactants (CS and MS) was very large, and the samples could be quickly heated to the reaction temperature in the high-quality fluidization state in the reactor. Next, the four-way valve was switched when the gas peak value returned to the baseline position. After entering the gas evenly mixed with argon and oxygen (8:2), the reaction began. An online mass spectrometer was used to detect the gaseous combustion products after injection and purification. When the gas curve was smooth, data collection was stopped, and the CO and CO_2 generated by the sample were analyzed. To ensure the accuracy of the experiment and reduce error in the experimental results, each experiment was repeated three times under the same conditions.

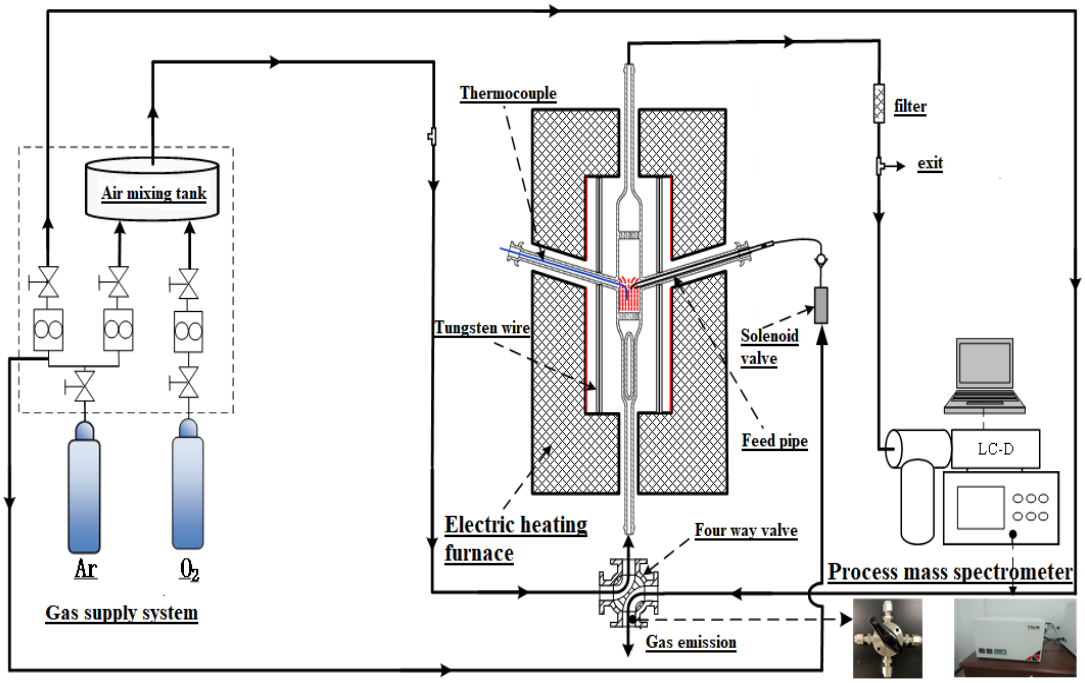

Figure 1. Isothermal rapid combustion test bench.

2.3. Kinetics Calculation Method

The isothermal method [**?**] was used to analyze the reaction kinetics of the biomass combustion process under isothermal conditions using the following equation, where T is the reaction temperature, f(x) is the differential reaction model function, and k(T) is a reaction rate constant that can be described by the Arrhenius equation.

$$\frac{dx}{dt} = k(T)f(x) \tag{1}$$

Taking the logarithms of both sides of Equation (1) gives:

$$\ln\left(\frac{dx}{dt}\right) = \ln k(T) + \ln f(x) \tag{2}$$

Integrating f(x) in Equation (1) results in:

$$G(x) = \int_0^x dx/f(x) = k(T)t \tag{3}$$

where G(x) is the integral form of the reaction mechanism function. The reaction rate constant k(T) can be expressed by the Arrhenius equation as:

$$k(T) = Aexp(-\frac{E}{RT}) \quad (4)$$

where A is the pre-exponential factor, E is the apparent activation energy, and R is the general gas constant. Taking the logarithms of both sides of Equation (4) gives:

$$lnk(T) = \ln(A) - E/RT \quad (5)$$

By replacing the common mechanism model function with Equation (3), the linear relationship between G(x) and reaction time t can be investigated at different temperatures, and the reaction activation energy and pre-exponential factor can be calculated according to the linear relationship in Equation (5). In Equation (3), T was set as the *x*-axis and G(x) as the *y*-axis. A line with the slope of the rate constant was fitted, then it was used to calculate the activation energy and refers to the pre-exponential factor by Equation (5).

The shrinking core model [**?**] assumes that the rate of gas diffusion is smaller and slower than the rate of the chemical reaction. Initially, the reaction only occurred on the particle surface; however, as the reaction progressed, the reaction gradually penetrated the core of the particle and became increasingly smaller.

The differential and integral forms of the mechanical function of the shrinking core model are as follows:

$$f(x) = (1-x)^{2/3} \quad (6)$$

$$G(x) = 1 - (1-x)^{2/3} \quad (7)$$

The shrinking core model introduced above starts the reaction from the particle surface and gradually moves inward, whereas the homogeneous model [**?**] does not discriminate between the inside and outside of the particle, with the reaction occurring on the whole particle. Moreover, the gas diffusion rate and chemical reaction rate in the reaction process did not differ and both were very fast. As the reaction progressed, the size of the model remained constant and the density changed uniformly, unlike in the shrinking core model.

The differential and integral forms of the mechanical function of the homogeneous model are as follows:

$$f(x) = 1 - x \quad (8)$$

$$G(x) = -\ln(1-x) \quad (9)$$

3. Results and Discussion

3.1. Determination of Test Parameters

3.1.1. Determination of Fluidization Gas Volume

The gas flow rate is an important factor for determining whether the fluidized bed has reached a stable fluidization state. Figure **??** shows the change curve of the carbon conversion rate over time during combustion with different fluidization gas volumes. The mixed-fuel mass was fixed at 12 $\pm$ 0.1 mg, and the samples were mixed very well before the experiments. An extremely low gas flow rate (200, 300 mL/min) caused the carbon conversion rate to be too low and lengthened the complete conversion time. With an increasing gas flow rate, the reaction rate increased, and the duration of complete conversion decreased. When the gas flow rate was greater than 500 mL/min, this effect gradually weakened, and the carbon conversion curve tended to coincide with the increase in the gas flow rate. These results indicate that a gas flow rate of 500 mL/min led to the best bed fluidization state and combustion reaction effect. Therefore, the gas flow rate was maintained at 500 mL/min in subsequent analyses.

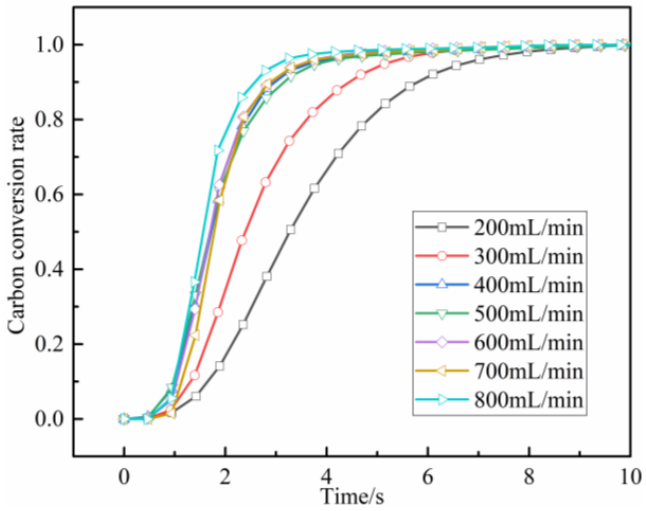

Figure 2. Effect of fluidizing gas flow rate on combustion reaction.

3.1.2. Variation in Temperature and Pressure in Micro-Fluidized Bed

To ensure that the combustion reaction in the micro-fluidized bed was an isothermal process, the temperature and pressure changes in the reactor during the reaction process were monitored in real-time using temperature and pressure sensors. Figure **??**a shows that at 550 °C, the temperature during combustion in the fluidized bed was maintained. The maximum fluctuation in temperature was 1 °C, indicating that the heat exchanged by the biomass injected into the fluidized bed had little effect on the temperature, and the fluidized bed test bench was isothermal, which is suitable for an isothermal rapid combustion reaction. Figure **??**b shows that the pressure during combustion in the fluidized bed fluctuated below a reference line, and each sudden change in pressure difference recovered quickly, indicating no significant impact of the instantaneous feed and that the experiment was carried out under relatively stable pressure. Thus, the fluidized bed test bed ensures a rapid combustion reaction under isothermal conditions and maintains the experimental pressure stability, supporting the reliability of our results.

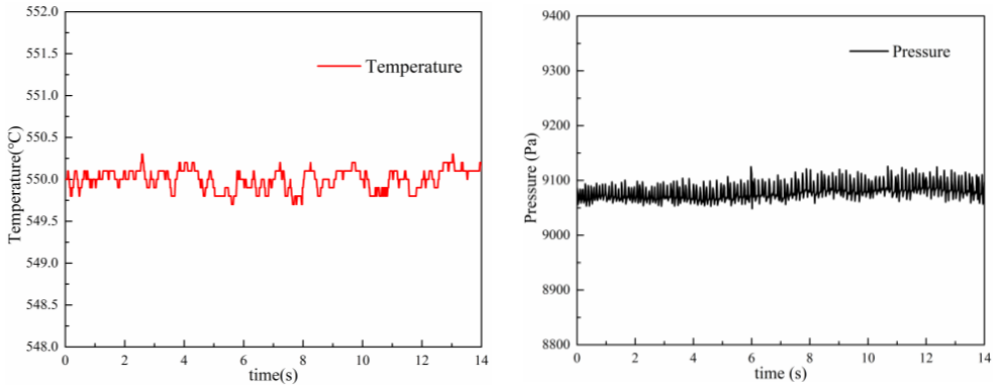

(**a**) Temperature (**b**) Pressure

Figure 3. Changes of temperature (**a**) and pressure (**b**) in fluidized bed during isothermal rapid combustion experiment.

3.1.3. Verification of Switching Atmosphere Stability

Figure **??** shows the change law of the gas release curve during sample injection into the reactor until the final combustion reaction was complete at 500 °C. There were two obvious peaks in the figure, and the entire combustion process was divided into two stages; the first peak was identified as the pyrolysis stage and the second peak as the coke combustion stage. Because the first stage was very quick and the second one was

much longer, the latter stage was much more important than the former one during co-combustion between MS and CS. The sample was injected into the reaction zone that had reached the set temperature, the pyrolysis reaction occurred, and a large amount of volatile matter was released to form the first peak, and these emissions could obviously impact the coke combustion. After the peak disappeared and the reference line became stable, the four-way valve was manually switched for a period of time. Throughout the process, the red curve representing O_2 showed no obvious fluctuations. Thus, manual switching of the four-way valve can achieve rapid and complete switching of the atmosphere. After switching the four-way valve, the coke combustion stage began with the introduction of a mixture containing oxygen, and the gas generated in this stage formed a second peak. The process lasted approximately 10 s and returned to the reference line after a short rise, indicating a rapid combustion reaction. Therefore, in this study, we only emphatically consider the mixed coke combustion process with the help of a four-way valve.

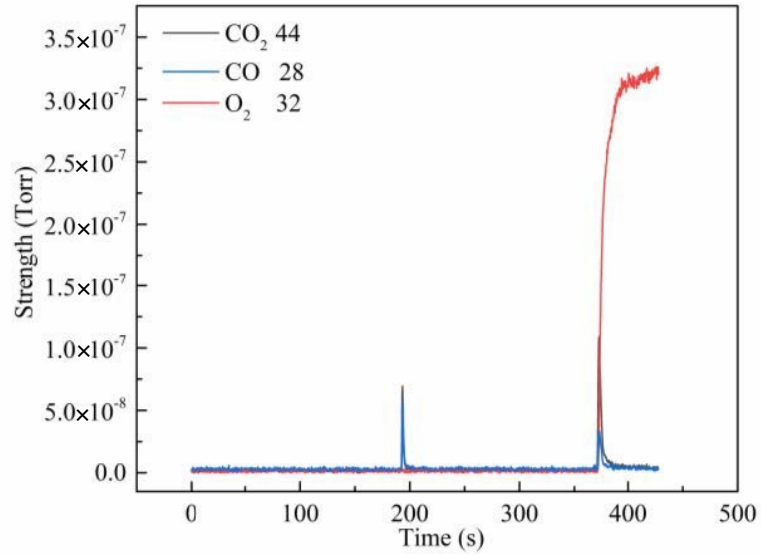

Figure 4. Gas release curve.

3.2. Analysis of Combustion Characteristics

3.2.1. Influence of Temperature on Carbon Conversion Rate in the Blending Process

Figure **??** shows the change in the carbon conversion rate over the reaction time in the isothermal rapid combustion reaction of samples with different proportions at 500 °C, 550 °C, 600 °C, and 650 °C. At each temperature, the carbon conversion rate increased with the reaction progress, finally reaching 1. A higher temperature was associated with a shorter time for the conversion rate to reach 1, which is more conducive to the reaction progress. Thus, a high temperature promotes combustion reactions and has a weaker effect on the reaction rate at a higher temperature. Xu et al. [**?**] evaluated the effect of temperature in the micro fluidized bed on the combustion of municipal solid waste coke, which is similar to the phenomenon in this paper. As shown in Figure **??**, as the reaction progressed, the reaction rate tended to first increase and then decrease; thus, the combustion process can be divided into two stages: Rapid combustion and burnout. After 3–4 s, the fuel was in the rapid combustion stage. After dehydration, the volatiles were analyzed and burned quickly. Because the carbon content of the mixed fuel was low, most coke was also burned in this stage. After reaching the burnout stage when most of the fuel was burned, the combustion rate decreased until being burned out because of the ash generated outside the fuel [**?**].

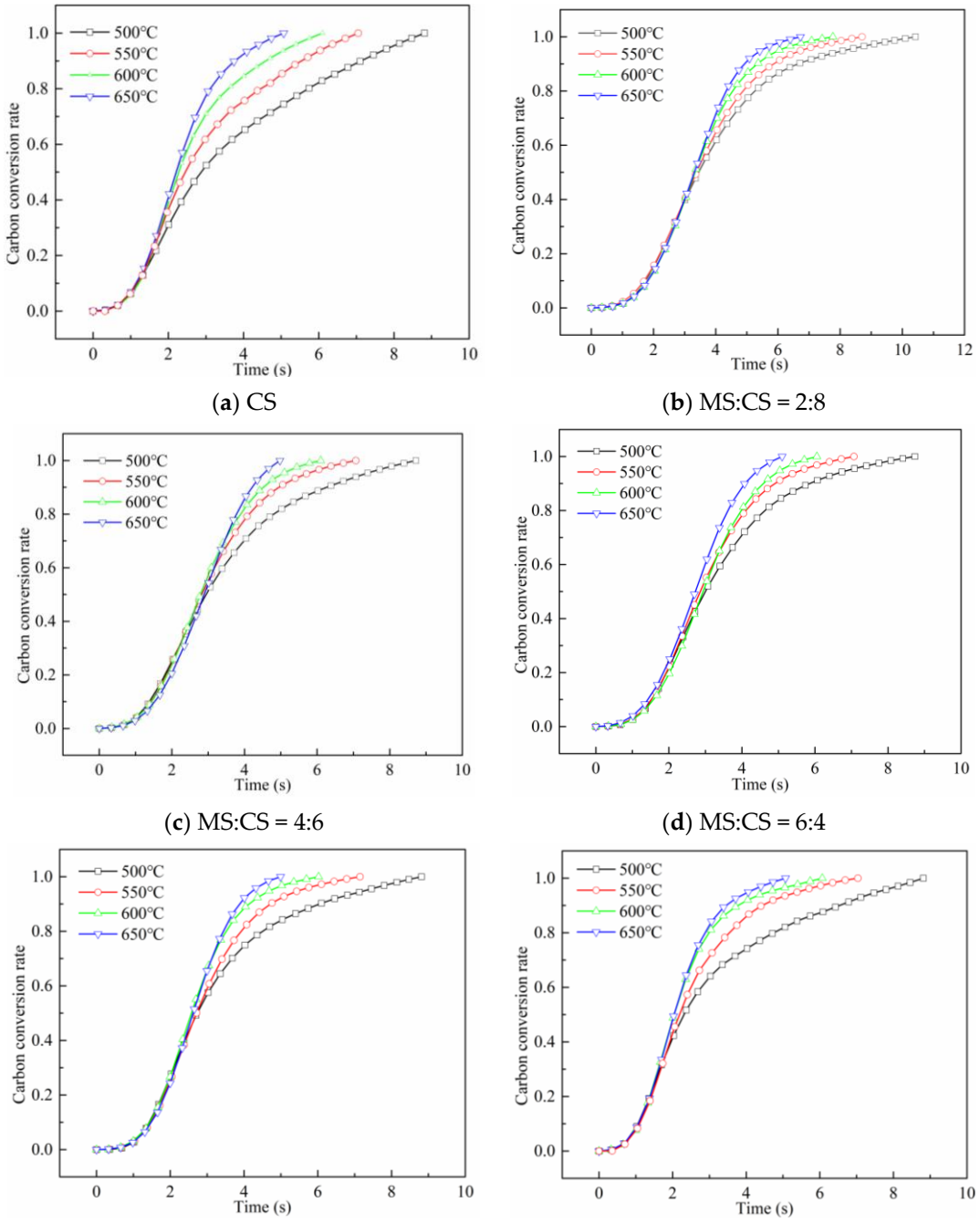

Figure 5. Variation of carbon conversion over time at different temperatures during mixed combustion for each mixing ratio.

3.2.2. Influence of Mixing Ratio on Carbon Conversion in Combustion Process

Figure **??** shows the change in the carbon conversion rate over time in the isothermal rapid combustion reaction of CS mixed with MS ratios of 20%, 40%, 60%, and 80% at different temperatures. The combustion performance of MS alone is poor, requiring the assistance of external energy. As an efficient clean energy source, CS can be co-fired with MS, which can effectively treat MS and make full use of the heat of MS and CS. At each temperature, with an increasing MS mixing ratio, the carbon conversion rate increased. According to industrial and elemental analyses, the carbon content and volatile matter of CS were higher than those of MS, indicating that CS has better fuel characteristics compared to MS. After adding MS, the fuel properties improved, possibly because the phosphorus

in MS inhibited the formation of low-melting-point alkali metal salts and the occurrence of the low-temperature eutectic phenomenon. The addition of MS weakens the bond-loss characteristics of MS in fluidized-bed combustion, thus improving the combustion behavior [**? ?**].

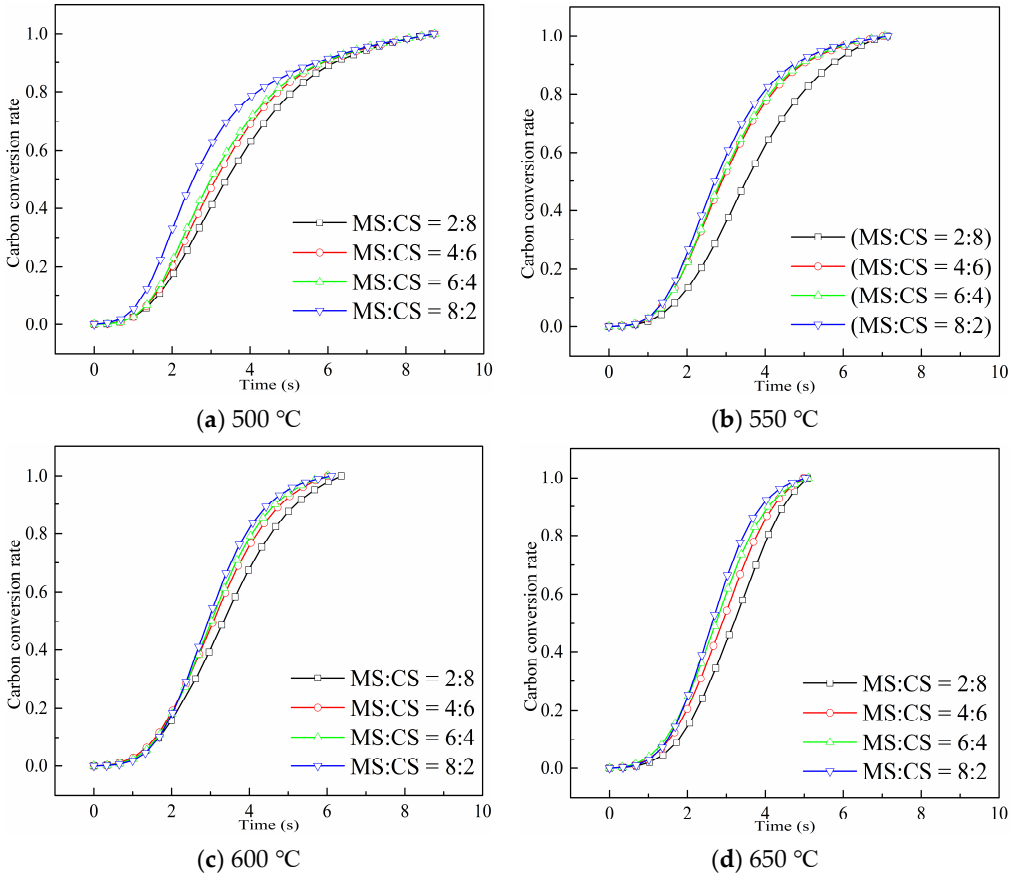

(**a**) 500 °C (**b**) 550 °C

(**c**) 600 °C (**d**) 650 °C

Figure 6. Variation of carbon conversion over time under different mixing ratios in mixed-combustion process at 500 °C, 550 °C, 600 °C, and 650 °C.

3.3. Isothermal Reaction Kinetics Analysis

3.3.1. Calculation of Shrinking Core Model

The reaction rate constant k (see Table **??**), determined using Equation (5), was used to calculate the activation energy (Ea) and refers to the pre-exponential factor (A) of the sample. The red curve in Figure **??** represents the fitting line of this model. The kinetic parameters are summarized in Table **??**, and the fitting degree (R^2) of each straight line was $\geq$0.96.

Table 3. Reaction rate constants calculated by shrinking core model.

	Temperature/°C	**500**	**550**	**600**	**650**
CS	k	0.08591	0.11616	0.14817	0.20559
	R^2	0.98584	0.99036	0.99247	0.99746
MS:CS = 2:8	k	0.11179	0.16155	0.20826	0.29304
	R^2	0.99642	0.99798	0.99713	0.9895
MS:CS = 4:6	k	0.09678	0.14326	0.19092	0.27587
	R^2	0.99355	0.99772	0.99967	0.994
MS:CS = 6:4	k	0.10358	0.14591	0.20158	0.25961
	R^2	0.99452	0.99647	0.99992	0.99919

Table 3. *Cont.*

	Temperature/°C	500	550	600	650
MS:CS = 8:2	k	0.09077	0.14035	0.1829	0.2664
	R^2	0.99006	0.99221	0.9935	0.99977
MS	k	0.07833	0.12017	0.12783	0.18094
	R^2	0.98834	0.99493	0.98912	0.99415

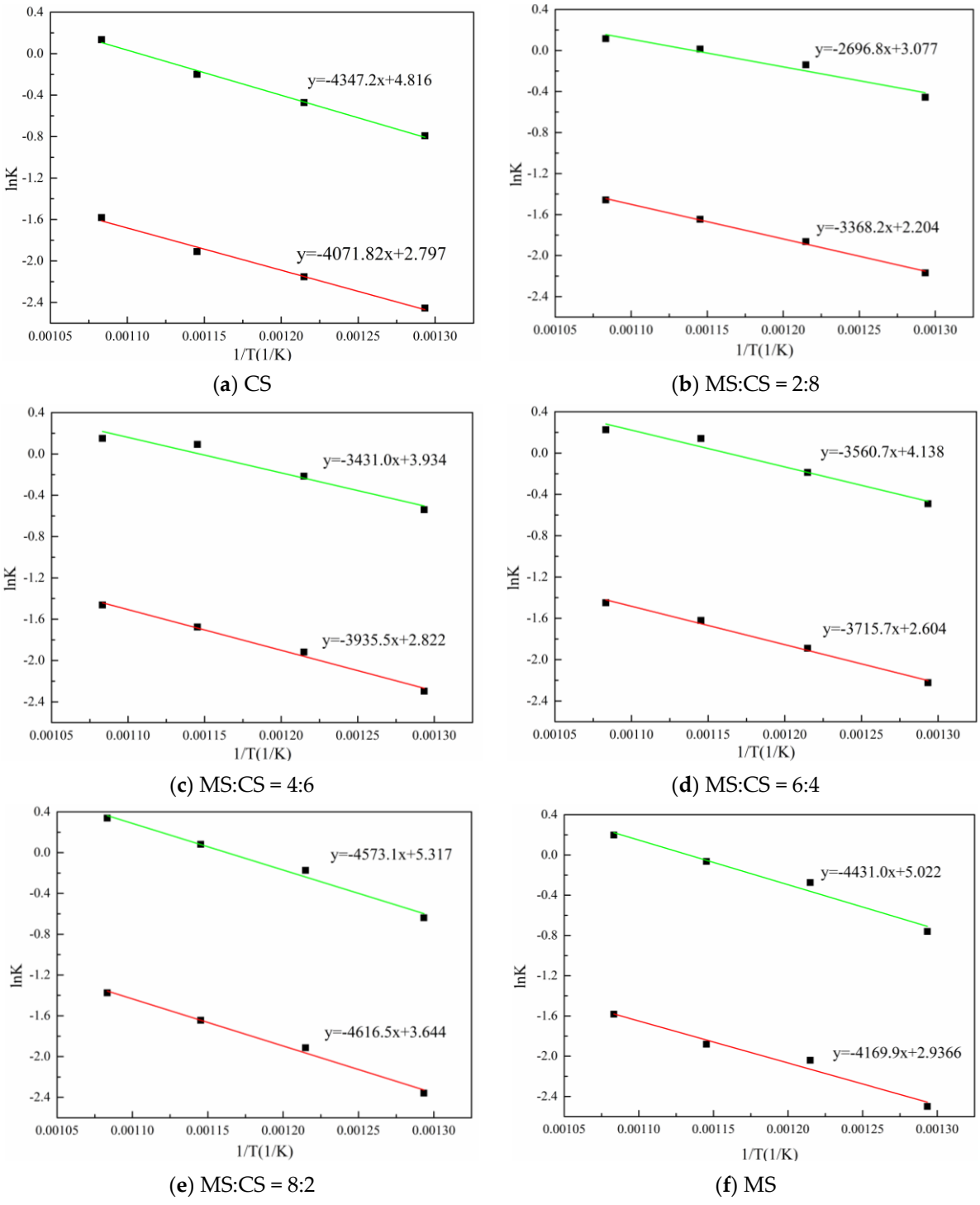

(**a**) CS (**b**) MS:CS = 2:8

(**c**) MS:CS = 4:6 (**d**) MS:CS = 6:4

(**e**) MS:CS = 8:2 (**f**) MS

Figure 7. Fitting results of combustion kinetic parameters of samples with different mixing ratios (The red line is fitting curve of shrinking core model, the green line is fitting curve of homogeneous model).

Table 4. Ea and A values calculated by shrinking core model.

	Ea/kJ mol^{-1}	**A/s^{-1}**	**R^2**
CS	33.85	16.39867	0.989
MS:CS = 2:8	28.00	9.062364	0.994
MS:CS = 4:6	30.89	16.80607	0.988
MS:CS = 6:4	32.72	13.51419	0.988
MS:CS = 8:2	38.38	38.23227	0.989
MS	34.67	18.85089	0.961

3.3.2. Calculation of Homogeneous Model

As with the homogeneous model, a straight line with a slope of the rate constant (k) was fitted, and the fitting degree of the fitting lines of different samples at different temperatures is summarized in Table **??**. The fitting degree of all lines was $\geq$0.96.

Table 5. Reaction rate constants calculated by homogeneous model.

	Temperature/°C	**500**	**550**	**600**	**650**
CS	k	0.46255	0.63893	0.83789	1.19941
	R^2	0.91501	0.93212	0.95998	0.9755
MS:CS = 2:8	k	0.76473	1.14119	1.46204	2.19227
	R^2	0.96963	0.95182	0.9574	0.97482
MS:CS = 4:6	k	0.63351	0.99822	1.37844	1.79162
	R^2	0.94241	0.96999	0.96482	0.95955
MS:CS = 6:4	k	0.70917	1.01372	1.38371	1.80037
	R^2	0.95928	0.97497	0.96829	0.97179
MS:CS = 8:2	k	0.5861	0.96177	1.29589	1.80544
	R^2	0.94657	0.98088	0.98392	0.97145
MS	k	0.47771	0.8488	0.94669	1.29181
	R^2	0.93937	0.96487	0.98912	0.98552

The homogeneous model was used to calculate the Ea and A values of the sample. The green curve in Figure **??** summarizes the fitting lines of the homogeneous model. The kinetic parameters are summarized in Table **??**, and the fitting degree of each line was $\geq$0.93.

Table 6. Ea and A values calculated by homogeneous model.

	Ea/kJ mol^{-1}	**A/s^{-1}**	**R^2**
CS	36.14	123.411	0.992
MS:CS = 2:8	22.42	21.684	0.937
MS:CS = 4:6	28.52	51.113	0.932
MS:CS = 6:4	29.60	62.707	0.953
MS:CS = 8:2	38.02	203.749	0.981
MS	36.84	151.643	0.967

3.3.3. Model Comparison and Analysis

A comparison of the data in Figure **??** and **????** showed that the fit of the shrinking core model was better than that of the homogeneous model, and the mixed-combustion process of MS and CS followed the law of the basic equation of combustion kinetics: $dx/dt = k(T)(1 - x)^{2/3}$. Therefore, the shrinking core model better described the isothermal combustion reaction behavior of mixed MS and CS. The calculated activation energy of the mixed combustion of MS and CS in different proportions was lower than that of single-fuel combustion. This is consistent with the increase in the reaction rate after adding MS, indicating a certain synergistic effect in the mixed combustion of MS and CS. The fit of the activation energy of the pure MS combustion reaction alone was 0.961, which may be

related to the high ash content in MS. The model assumes that the ash layer formed on the surface reacts, and the reaction gradually penetrates the interior. Particles with a high ash content prevent diffusion of the reaction gas to the core, because of which the combustion of MS did not conform with the shrinking core model [**?**].

4. Conclusions

The conclusions of this study are as follows: Firstly, the isothermal combustion process of MS and CS could be divided into two stages: Rapid burning and burnout. As the temperature of the samples under the same blending ratio increased, the time to reach the same carbon conversion rate gradually decreased, indicating that a high temperature promoted the combustion reaction. Furthermore, a comparison of different blending ratios at the same temperature showed that when the MS blending amount was 20%, the carbon conversion rate was increased, which was more conducive to combustion. Secondly, the calculation of the isothermal kinetics of the homogeneous and shrinking core models showed that the activation energies calculated using the two models did not significantly differ. However, the fitting degree of the shrinking core models was better than that of the homogeneous model, and the calculated pre-exponential factor was more stable. Therefore, the shrinking core models are more suitable for describing the isothermal kinetic combustion calculation in this study. Finally, as the amount of added MS into CS was increased, the activation energy of each mixed sample decreased and was lower than that of a single fuel. Thus, there was a synergistic effect for the mixed combustion of MS and CS; when the MS level was 20%, the activation energy reaches the lowest value, which was most conducive to the combustion of materials.

The mixed combustion of solid waste is a prospective technology. However, little research has occurred regarding the combustion characteristics and reaction kinetics of MS and CS. To enable the rational utilization of CS resources and disposal of MS, we co-combusted CS and MS, examined the characteristics of this co-combustion by analyzing the conversion rate and reaction kinetics, and evaluated the effect of adding MS on the combustion of mixed fuels. In future studies, we intend to explore the potential secondary reactions and synergistic effects during mixed combustion between CS and MS. Meanwhile, we also plan to study the migration characteristics of various heavy metals, promoting the industrial application of mixed-combustion technology.

Author Contributions: Conceptualization and methodology, S.G. (Shengjie Guo), S.G. (Shuai Guo), and J.T.; validation, Z.Y. and S.D.; writing—original draft preparation, S.G. (Shengjie Guo); writing—review and editing, S.D. and Y.W. All authors have read and agreed to the published version of the manuscript.

Funding: This research was funded by the Heilongjiang Bayi Agricultural University Support Program for San Heng San Zong (Grant No. TDJH202005).

Institutional Review Board Statement: Not applicable.

Informed Consent Statement: Not applicable.

Data Availability Statement: Not applicable.

Conflicts of Interest: The authors declare no conflict of interest.

References

1. Zou, C.N.; Pan, S.Q.; Zhao, Q. On the connotation, challenge and significance of China's "energy independence" strategy. *Pet. Explor. Dev.* **2020**, *47*, 449–462. [CrossRef]
2. Chen, Y.Q.; Sun, S.Q.; Jin, J.; Wang, L. Introduction to Technique of Incineration for Municipal Sludge. In Proceedings of the 2nd International Conference on Asian-European Environmental Technology and Knowledge Transfer, Hefei, China, 5–6 June 2008.
3. Cao, Y.B. Application Status and Development Strategies of Biomass Energy in China. In Proceedings of the 2nd International Conference on Energy, Environment and Sustainable Development (EESD 2012), Jilin, China, 12–14 October 2012. [CrossRef]
4. He, J.X.; Zhu, R.Q.; Lin, B.Q. Prospects, obstacles and solutions of biomass power industry in China. *J. Clean Prod.* **2019**, *237*, 117783. [CrossRef]

5. Ma, L.L.; Wang, T.J.; Liu, Q.Y.; Zhang, X.H.; Ma, W.C.; Zhang, Q. A review of thermal-chemical conversion of lignocellulosic biomass in China. *Biotechnol. Adv.* **2012**, *30*, 859–873. [CrossRef] [PubMed]
6. Zhang, K.H.; Zhang, K.; Cao, Y.; Pan, W.P. Co-combustion characteristics and blending optimization of tobacco stem and high-sulfur bituminous coal based on thermogravimetric and mass spectrometry analyses. *Bioresour. Technol.* **2013**, *131*, 325–332. [CrossRef]
7. Huang, J.L.; Liu, J.Y.; Kuo, J.H.; Xie, W.M.; Zhang, X.C.; Chang, K.; Buyukada, M.; Evrendilek, F. Kinetics, thermodynamics, gas evolution and empirical optimization of (co-) combustion performances of spent mushroom substrate and textile dyeing sludge. *Bioresour. Technol.* **2019**, *280*, 313–324. [CrossRef]
8. Sahu, S.G.; Chakraborty, N.; Sarkar, P. Coal-biomass co-combustion: An overview. *Renew. Sustain. Energy Rev.* **2014**, *39*, 575–586. [CrossRef]
9. Liu, H.M.; Wang, Y.C.; Zhao, S.L.; Hu, H.Y.; Cao, C.Y.; Li, A.J.; Yu, Y.; Yao, H. Review on the current status of the co-combustion technology of organic solid waste (OSW) and coal in China. *Energy Fuels* **2020**, *34*, 15448–15487. [CrossRef]
10. Wang, G.W.; Zhang, J.L.; Shao, J.G.; Ren, S. Characterisation and model fitting kinetic analysis of coal/biomass co-combustion. *Thermochim. Acta* **2014**, *591*, 68–74. [CrossRef]
11. Qian, X.J.; Lee, S.; Chandrasekaran, R.; Yang, Y.L.; Caballes, M.; Alamu, O.; Chen, G.M. Electricity evaluation and emission characteristics of poultry litter co-combustion process. *Appl. Sci.* **2019**, *9*, 4116. [CrossRef]
12. Ryu, C.; Yang, Y.B.; Khor, A.; Yates, N.E.; Sharifi, V.N.; Swithenbank, J. Effect of fuel properties on biomass combustion: Part I. Experiments—Fuel type, equivalence ratio and particle size. *Fuel* **2006**, *85*, 1039–1046. [CrossRef]
13. Wang, X.; Ren, Q.Q.; Li, W.; Li, H.Y.; Li, S.Y.; Lu, Q.G. Nitrogenous gas emissions from coal/biomass co-combustion under a high oxygen concentration in a circulating fluidized bed. *Energy Fuels* **2017**, *31*, 3234–3242. [CrossRef]
14. Qin, H.; Yue, Y.K.; Zhang, L.D.; Liu, Y.Y.; Chi, M.S.; Liu, H.P.; Wang, Q.; Liu, B. Study on co-combustion kinetics of oil shale sludge and semicoke. *Energy Fuels* **2016**, *30*, 2373–2384. [CrossRef]
15. Yin, Y.S.; Yang, B.M.; Yin, J.; Tian, H.; Zhang, W.; Cheng, S.; Hu, Z.M.; Xu, H.F. Kinetic analysis of co-firing of corn stalk and paper sludge using model-fitting and model-free methods. *J. Energy Resour. Technol. Trans. ASME* **2020**, *142*, 042301. [CrossRef]
16. Wang, J.F.; Wen, L.; Chen, Y.; Han, H.C. Study on The Combustion Characteristics and Kinetics of Biomass and Coal Char Blended Fuels. In Proceedings of the 7th International Conference on Renewable Energy Research and Applications (ICRERA), Paris, France, 14–17 October 2018.
17. Tian, H.; Liao, Z.Z. Co-combustion characteristics and kinetics of coal, oil shale and petroleum coke. *Clean Coal Technol.* **2017**, *23*, 60–64, 68. (In Chinese)
18. Dai, R.J.; Song, J.; Zhang, X.L. Study of the combustion characteristics of coal gangue mixed with coal from Huaibei mining area. *J. Anhui Inst. Archit. Ind.* **2013**, *21*, 41–45. (In Chinese) [CrossRef]
19. Wang, H.; Guo, S.; Liu, D.Y.; Guo, Y.Z.; Gao, D.Y.; Sun, S.Z. A dynamic study on the impacts of water vapor and impurities on limestone calcination and CaO sulfurization processes in a microfluidized bed reactor analyzer. *Energy Fuels* **2016**, *30*, 4625–4634. [CrossRef]
20. Guo, S.; Yu, S.X.; Che, D.Y.; Liu, H.P.; Sun, B.Z. Migration characteristics of heavy metals during co-combustion of dehydrated sludge with straw. *J. Fuel Chem. Technol.* **2022**, *50*, 283–294. [CrossRef]
21. Yu, J.; Zeng, X.; Zhang, J.W.; Zhong, M.; Zhang, G.Y.; Wang, Y.; Xu, G.W. Isothermal differential characteristics of gas-solid reaction in micro-fluidized bed reactor. *Fuel* **2013**, *103*, 29–36. [CrossRef]
22. Melchiori, T.; Canu, P. Improving the quantitative description of reacting porous solids: Critical analysis of the shrinking core model by comparison to the generalized grain model. *Ind. Eng. Chem. Res.* **2014**, *53*, 8980–8995. [CrossRef]
23. Teng, Y.Y.; Liu, Y.Z.; Liu, Q.S.; Li, C.Q. Macerals of Shengli lignite in inner Mongolia of China and their combustion reactivity. *J. Chem.* **2016**, *2016*, 2513275. [CrossRef]
24. Xu, M.; Zhu, X.Q.; Li, X.; Hu, Z.Z.; Huang, Y.; Xia, A.O.; Yao, H. Investigation of the combustion behaviors and kinetic modelling of municipal solid waste char under isothermal conditions using a micro-fluidized bed. *J. Environ. Chem. Eng.* **2021**, *9*, 105984. [CrossRef]
25. Sun, W.Y.; Wang, L.M.; Ma, C.; Ma, Y.R.; Lv, Y.; Feng, K. Combustion and kinetics of straw and sludge briquette fuel. *Biomass Chem. Eng.* **2017**, *51*, 53–58. (In Chinese)
26. Li, L.N.; Ren, Q.Q.; Li, S.Y.; Lu, Q.G. Effect of phosphorus on the behavior of potassium during the co-combustion of wheat straw with municipal sewage sludge. *Energy Fuels* **2013**, *27*, 5923–5930. [CrossRef]
27. Ren, Q.Q.; Li, L.N. Co-combustion of agricultural straw with municipal sewage sludge in a fluidized bed: Role of phosphorus in potassium behavior. *Energy Fuels* **2015**, *29*, 4321–4327. [CrossRef]
28. Zang, X.J.; Wang, X.Y.; Guo, L.Y.; Du, G. Fitting analysis of different models of CO_2 gasification kinetics of Shenmu long flame coal. *Clean Coal Technology* **2020**, *26*, 147–152. (In Chinese)